Lithos 318–319 (2018) 47–59

Contents lists available at ScienceDirect

Lithos

journal homepage: www.elsevier.com/locate/lithos

# Petrogenesis of Late Paleozoic diorites and A-type granites in the central Eastern Tianshan, NW China: Response to post-collisional extension triggered by slab breakoff

Long Du [a,b,c], Xiaoping Long [a,*], Chao Yuan [b], Yunying Zhang [b], Zongying Huang [b], Min Sun [d], Wenjiao Xiao [e]

[a] State Key Laboratory of Continental Dynamics, Department of Geology, Northwest University, Xi'an 710069, China
[b] State Key Laboratory of Isotope Geochemistry, Guangzhou Institute of Geochemistry, Chinese Academy of Sciences, Guangzhou 510640, China
[c] College of Geological Science and Engineering, Shandong University of Science and Technology, Qingdao 266590, China
[d] Department of Earth Sciences, The University of Hong Kong, Pokfulam, Road, Hong Kong, China
[e] State Key Laboratory of Lithospheric Evolution, Institute of Geology and Geophysics, Chinese Academy of Sciences, Beijing 100029, China

ARTICLE INFO

*Article history:*
Received 21 March 2018
Accepted 3 August 2018
Available online 7 August 2018

*Keywords:*
A-type granite
Post-collisional
Slab breakoff
Eastern Tianshan
Central Asian Orogenic Belt

ABSTRACT

Geological evolution of the Eastern Tianshan in the Late Paleozoic is significant to understanding the multiple accretions and final formation of the southern Central Asian Orogenic Belt. Here, we report new whole-rock geochemical and Sr–Nd isotopic data, and in situ zircon U–Pb ages for three typical A-type granitic intrusions (syenogranite, K-feldspar granite and monzonitic granite) and one dioritic pluton in the central Eastern Tianshan, NW China, in order to constrain their petrogenesis, tectonic setting and geodynamic evolution. Zircon LA-ICP-MS U–Pb ages indicate that the syenogranites and K-feldspar granites were both formed during a short time interval in the Early Permian (284–286 Ma), whereas the diorites were crystallized at 293 ± 6 Ma. The monzonitic granites were generated at 307 ± 3 Ma, earlier than the other two granitic intrusions. The three kinds of granites (syenogranite, K-feldspar granite and monzonitic granite) have high HFSE, HREE and Y/Nb ratios (1.68–2.84), and remarkably low Sr and Ba contents, with the absence of aluminium-rich minerals and show metaluminous to weakly peraluminous natures, indicating geochemical characteristics of aluminous $A_2$-type granites. These granites show negative $\varepsilon_{Nd}(t)$ (−3.32 to −4.40) values and Mesoproterozoic two stage Nd model ages ($T^2_{DM}$ = 1.36 to 1.43 Ga), which suggest a relatively old crustal source for these rocks. The Sr–Nd isotopic compositions imply that the Mesoproterozoic metamorphic basement of the Central Tianshan Block can be considered as a potential magmatic source for these aluminous $A_2$-type granites. In addition, they have geochemical characteristics similar to the experimental melt that was derived from partial melting of crustal metaigneous rocks at the depth of middle to lower crust levels. Therefore, the granites were most likely produced by partial melting of metaigneous rocks in a post-collisional extensional setting. The diorites have low $SiO_2$ and high MgO, with uniform $(^{87}Sr/^{86}Sr)_i$ values (~0.7055), negative $\varepsilon_{Nd}(t)$ values (−4.11 to −4.59) and Mesoproterozoic two stage Nd model ages ($T^2_{DM}$ = 1.41 to 1.45 Ga). They have higher Ti/Zr (42.8–46.7) and Ti/Y (280–359) ratios than continental crust and show negative Nb-Ta-Ti anomalies, which can be explained by partial melting of a relatively fertile mantle modified by old crustal materials of the Central Tianshan Block. The formation of the dioritic pluton was induced by an upwelling asthenosphere in an extensional geodynamic setting. Based on the zircon saturation temperatures of these A-type granites and the distribution of Late Carboniferous to Early Permian mantle-derived intrusions, a slab breakoff model is suggested to interpret the formation of the studied A-type granites and diorites. We infer that the slab breakoff was initiated in the Late Carboniferous and ended in the Early Permian.



## 1. Introduction

The Central Asian Orogenic Belt (CAOB), also known as "the modified Altaids" in the literature (Sengör et al., 1993; Xiao et al., 2015), which is one of the largest accretionary orogenic belts in the world, lying between the European craton to the west, the Siberian craton to the north, and the Tarim and North China cratons to the south (Fig. 1a; Sengör et al., 1993; Xiao et al., 2015). It was experienced long-lived evolution involving multiple accretions of island arcs, accretionary prisms, seamounts and microcontinents within the Paleo-Asian Ocean (Windley et al., 1990; Sengör et al., 1993; Kröner et al.,

* Corresponding author.
*E-mail address:* longxp@nwu.edu.cn (X. Long).

https://doi.org/10.1016/j.lithos.2018.08.006
0024-4937/

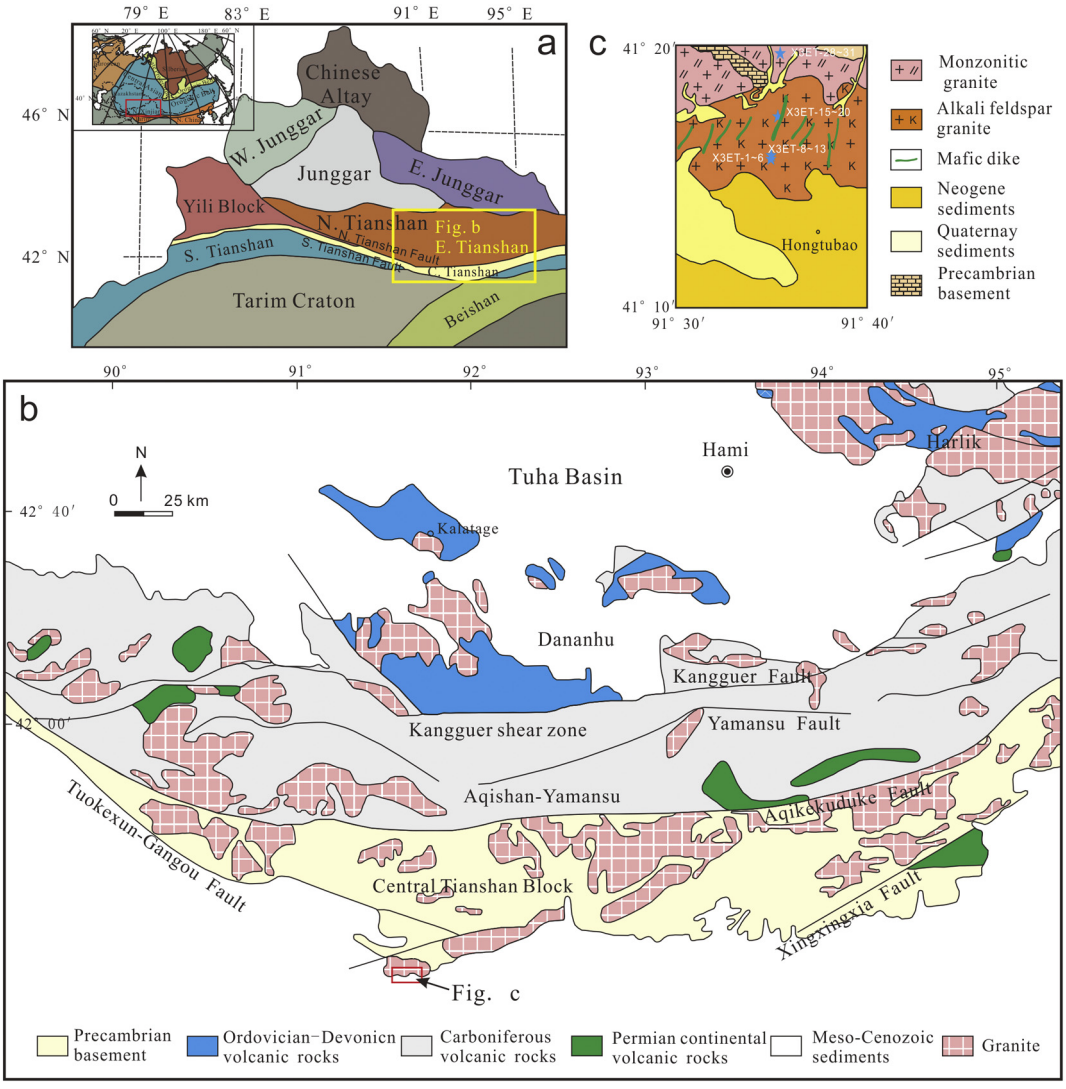


**Fig. 1.** (a) Tectonic sketch map of the Central Asia Orogenic Belt and North Xinjiang (after Gao et al., 2009, 2011). (b) Geological map of the Eastern Tianshan (after Li et al., 2016). (b) Simplified geological map of sampling sites in the eastern Central Tianshan Block (modified after BGMRXUAR, 1993).

2007; Xiao et al., 2015). The tectonic framework of the CAOB is generally regarded as a result of the final formation of the Kazakhstan and Tuva-Mongol oroclines along the Irtysh shear Zone as well as the convergence of the Tarim and North China cratons along the South Tianshan-Solonker suture zone (Sengör et al., 1993; Xiao et al., 2015). The continuance and architecture of the two oroclines are key issues of the geological evolution of the CAOB and drew many attentions to the domestic and international researchers (Windley et al., 1990; Sengör et al., 1993; Kröner et al., 2007; Xiao et al., 2015).

Situated in the southern part of the CAOB, the Tianshan Orogenic Belt represents the final collision zone between the Tarim Craton and the Junggar Block, the tectonic evolution of the Tianshan belt is believed to have a genetic link with the bending of the Kazakhstan orocline and the subduction of ancient oceanic plates (Fig. 1a; Gao et al., 1998, 2009, 2011; Gao and Klemd, 2003; Charvet et al., 2007; Han et al., 2010, 2011, 2015, 2016; Wang et al., 2010, 2011, 2018a; Xiao et al., 2015; Zhang et al., 2016). Although the Tianshan Orogenic Belt is characterized by voluminous multi-stage granitic intrusions and mainly Early Permian mafic–intermediate intrusions, the tectonic setting for the magmatism is still a matter of debate in the Late Paleozoic, especially the east segment of the Chinese Tianshan, which hinder the clues to understand the final formation of the southern CAOB (Cai et al., 2018; Deng et al., 2015; Du et al., 2018a; Gao et al., 1998, 2009, 2011; Han et al., 2010, 2011, 2015, 2016; Qin et al., 2011; Wang et al., 2010, 2011, 2018a, 2018b; Zhang et al., 2016; Zhao et al., 2018).

Generally, the temporal and spatial distribution of Late Paleozoic granitic rocks and mafic–intermediate rocks have genetic relationships with the geodynamic processes (Tang et al., 2014; Wang et al., 2014; Yuan et al., 2010), which has been well tested in the Western Tianshan (e.g. Cao et al., 2017; Han and Zhao, 2017; Wang et al., 2009). Therefore, in this contribution we present new whole-rock geochemical and Sr–Nd isotopic data and zircon U–Pb ages for representative Late Carboniferous to Early Permian dioritic and A-type granitic intrusions in the central Eastern Tianshan, in order to constrain the source and genetic relationship between them and unravel the Late Paleozoic geodynamic evolution of the Eastern Tianshan and the final formation of the southern CAOB.

## 2. Geological background

The Chinese Tianshan Orogenic Belt can be geographically divided into the eastern and western segments roughly along the Urumqi-Korla road, which experienced different evolution during the Paleozoic time (Gao et al., 2009; Windley et al., 1990). The Eastern Tianshan is a ca. 1500 km long and 300 km wide orogenic belt in the southern CAOB and lying between the eastern Junggar to the north and the

Tarim Carton to the south (Fig. 1b; Charvet et al., 2007, 2011; Huang et al., 2017). It is tectonically divided into three tectonic belts from north to south, namely the North Tianshan, the Central Tianshan, and the South Tianshan, separated by the North Tianshan fault and the South Tianshan fault (Fig. 1a; Charvet et al., 2007; Gao et al., 2009; Huang et al., 2017).

The North Tianshan comprises of Harlik, Dananhu, Kangguer and Yamansu belts from north to south (Fig. 1b). The Harlik belt is mainly composed of Ordovician to Silurian clastics, tuffs, volcaniclastics, and Devonian to Carboniferous volcanic rocks and flysch sediments (Du et al., 2018a; Yuan et al., 2010). The Dananhu belt is overlain by Ordovician to Carboniferous volcanic and pyroclastic rocks, with accretionary complexes composed of turbidite, basalt, chert, and ultramafic rock (Qin et al., 2002). Based on the combination of regional geology and recently studies on Early Paleozoic high-Mg andesites and arc-type granitic plutons in these area (Du et al., 2018a; Zhang et al., 2017 and references therein), the Harlik-Dananhu belt were considered as a result of north-dipping subduction of the Kangguer oceanic lithosphere prior to the Late Ordovician (Du et al., 2018a). Contact by the Kangguer fault with the Dananhu arc to the north, the Kangguer belt mainly include Devonian to Carboniferous sedimentary and volcanic rocks, which consists of conglomerate, sandstone, siltstone, bioclastic limestone, basalt and andesite (BGMRXUAR, 1993; Wang et al., 2014). Ophiolites with Paleozoic ages (330 and 494 Ma) (Li et al., 2008; Liu et al., 2016) along the Kangguer fault represent remnants of the Kangguer oceanic plate. To the south, the Aqishan-Yamansu belt mainly contains two marine units: the Early Carboniferous Yamansu Formation and the Late Carboniferous Tugutublak Formation. The sedimentary rocks of the Yamansu and Tugutublak Formations were intruded by numerous arc-related Late Paleozoic granitoids (Du et al., 2018b; Wang et al., 2018b; Zhao et al., 2018).

The Central Tianshan Block is separated from the Aqishan-Yamansu belt to the north by the Aqikekuduke fault (Fig. 1b). It predominantly consists of Precambrian–Mesozoic magmatic and sedimentary rocks (He et al., 2014; Huang et al., 2017; Lei et al., 2011; Li et al., 2016; Liu et al., 2004; Zhang et al., 2016). The Precambrian basement rocks were divided into the Tianhu, Kawabulake and Xingxingxia groups, most of them have experienced green-schist to amphibolite facies metamorphism and are unconformably overlain by or in fault contact with Paleozoic strata (Hu et al., 1998; Zhang et al., 2016). The basement is mainly composed of gneisses and migmatites overlain by Precambrian metasedimentary covers including clastic rocks, limestones and quartzites (1458–730 Ma) (e.g. Huang et al., 2017). Early Paleozoic to Early Mesozoic ultramafic to felsic volcanic rock, granitoid, graywacke and flysch rock are exposed in the Central Tianshan Block (Ma et al., 2015; Zhang et al., 2016).

The South Tianshan belt is bounded between the Central Tianshan Block and the northern margin of the Tarim Craton (Fig. 1a). It comprises the deformed Paleozoic sedimentary rocks, volcanics and volcaniclastic, associated with Ordovician to Carboniferous ophiolites, and Devonian to Carboniferous high-pressure metamorphic rocks (Huang et al., 2017). These sediments and volcanics assemblage is different from the arc-related volcanic rocks in the Central Tianshan Block. The South Tianshan belt was proposed to be a Paleozoic back-arc basin (Charvet et al., 2007) or a paleo-ocean (named the South Tianshan Ocean) that existed between Tarim and the Central Tianshan Belt (Windley et al., 1990).

## 3. Sampling and petrography

In this study, dioritic and granitic samples were collected from plutons near the Hongtubao area (Fig. 1c and Fig. 2a–d). These plutons are located on the south margin of the Central Tianshan Block and intruded into the Precambrian basement (Fig. 1b, c). Most of the monzonitic granitic plutons were distributed in the northern part of the Central Tianshan Block (Fig. 1c). The K-feldspar granitic pluton and syenogranitic pluton were interacted with each other (Fig. 2a). Also, the dioritic pluton was intruded by the K-feldspar granites (Fig. 2c).

The diorite samples have medium-grained granular with equigranular texture. They mainly consist of plagioclase (30–35%), K-feldspar (30–35%) and amphibole (20–25%), with minor pyroxene (~5%), biotite (~5%) and accessory minerals (<5%) (Fig. 2e, f). Most pyroxene is replaced by igneous amphibole, and some amphiboles and biotites exhibit chloritization (Fig. 2e, f). The syenogranites are medium- to coarse-grained texture (Fig. 2g). They are composed of quartz (25–30%), orthoclase (25–30%), K-feldspar (10–15%), plagioclase (~10%), and biotite (~5%), with minor accessory minerals (<5%) (Fig. 2g). The K-feldspar granite samples mainly consist of quartz (35–40%), K-feldspar (35–40%), plagioclase (10–15%), amphibole (~5%), and biotite (~5%), with minor accessory minerals (<5%) (Fig. 2h). The monzonitic granites are gray color with subhedral granular texture and mainly include euhedral plagioclase (30–35%), K-feldspar (20–25%), and anhedral quartz (30–35%), with minor amphibole (~5%), biotite (~5%) and accessory minerals (<5%) (Fig. 2d, i).

## 4. Analytical results

Detailed analytical methods are described in Appendix and the results are listed in Supplementary tables.

### 4.1. Zircon U–Pb age

Zircon grains from the diorite sample (X3ET-15) are mostly dark in color, and stubby to prismatic in shape in CL images (Fig. 3a). They have variable Th (122–2236 ppm) and U (437–1843 ppm) contents and possess moderate to high Th/U ratios (0.14–1.38) (Supplemental Table S1), suggesting an igneous origin (Wu and Zheng, 2004). We have analyzed twenty-three zircons, of which one analysis (No. 11) plots above the Concordia curve and gives an apparent $^{206}Pb/^{238}U$ age of 453 ± 5 Ma. The other twenty-two zircons yield a weighted $^{206}Pb/^{238}U$ mean age of 293 ± 6 Ma (MSWD = 5.2) (Fig. 3a), which is interpreted as the formation age of the dioritic pluton.

Zircons from the syenogranite sample (X3ET-01) have high transparency and exhibit typical characteristics of igneous zircons with oscillatory zoning (Fig. 3b). They have moderate Th (90–732 ppm) and U (213–1506 ppm) contents with moderate Th/U ratios (0.34–0.67) (Supplemental Table S1). Twenty grains were analyzed and yield $^{206}Pb/^{238}U$ ages ranging from 261 Ma to 300 Ma, which yield a weighted mean $^{206}Pb/^{238}U$ age of 286 ± 4 Ma (MSWD = 1.8) (Fig. 3b). This age is interpreted as the crystallization age of the syenogranitic pluton.

Zircon grains from the K-feldspar granite sample (X3ET-08) show similar shapes to those from the syenogranitic pluton and also exhibit typical characteristics of igneous zircons with oscillatory zoning. Twenty zircons were analyzed and yield a weighted mean $^{206}Pb/^{238}U$ age of 284 ± 2 Ma (MSWD = 0.48) (Fig. 3c), which is considered to be the formation age of the K-feldspar granitic pluton.

Zircons from the monzonitic granite sample (X3ET-28) are euhedral, prismatic crystals with length/width ratios 2 to 3, and have concentric oscillatory zoning in CL images in good agreement with igneous zircons (Fig. 3d). They are characterized by relatively low Th (29–232 ppm) and U (91–462 ppm) contents, with Th/U ratios (0.23–0.48) (Supplemental Table S1). Twenty analyses form a tight cluster and yield a weighted mean age of 307 ± 3 Ma (MSWD = 0.26) (Fig. 3d), indicating that the monzonitic granitic pluton was formed in the Late Carboniferous.

### 4.2. Whole-rock geochemistry

#### 4.2.1. Diorites

The dioritic samples display low $SiO_2$ (50.8–55.2 wt%), high MgO (4.30–5.30 wt%), $Fe_2O_3^T$ (8.83–9.48 wt%) and Mg# (49–53) (Supplemental Table S2). They are characterized by moderate $TiO_2$

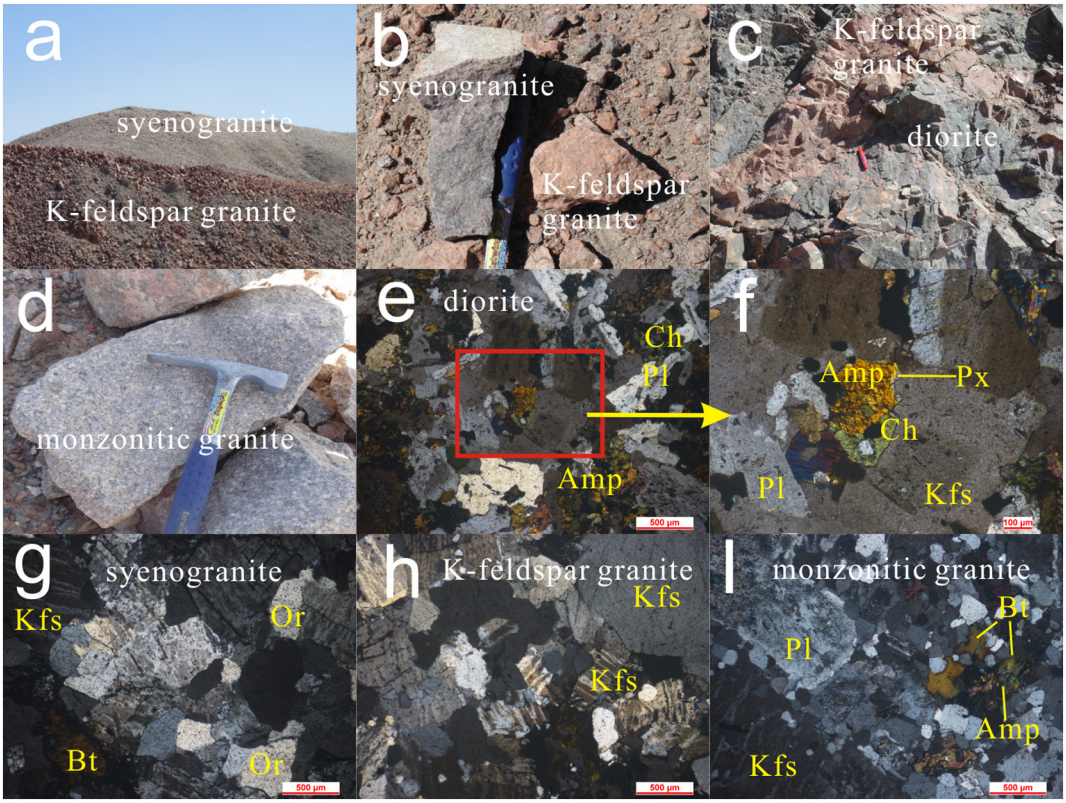


**Fig. 2.** (a)–(d) Field photos of the Late Paleozoic dioritic and granitic plutons in the eastern Central Tianshan Block. (e)–(i) Textural characteristics of the Late Paleozoic rocks as seen in thin-section under cross-polarized light. Mineral abbreviations: Amp — Amphibole, Bt — Biotite, Ch — Chlorite, Kfs — K-feldspar, Or — Orthoclase, Pl — Plagioclase, and Px — Pyroxene.

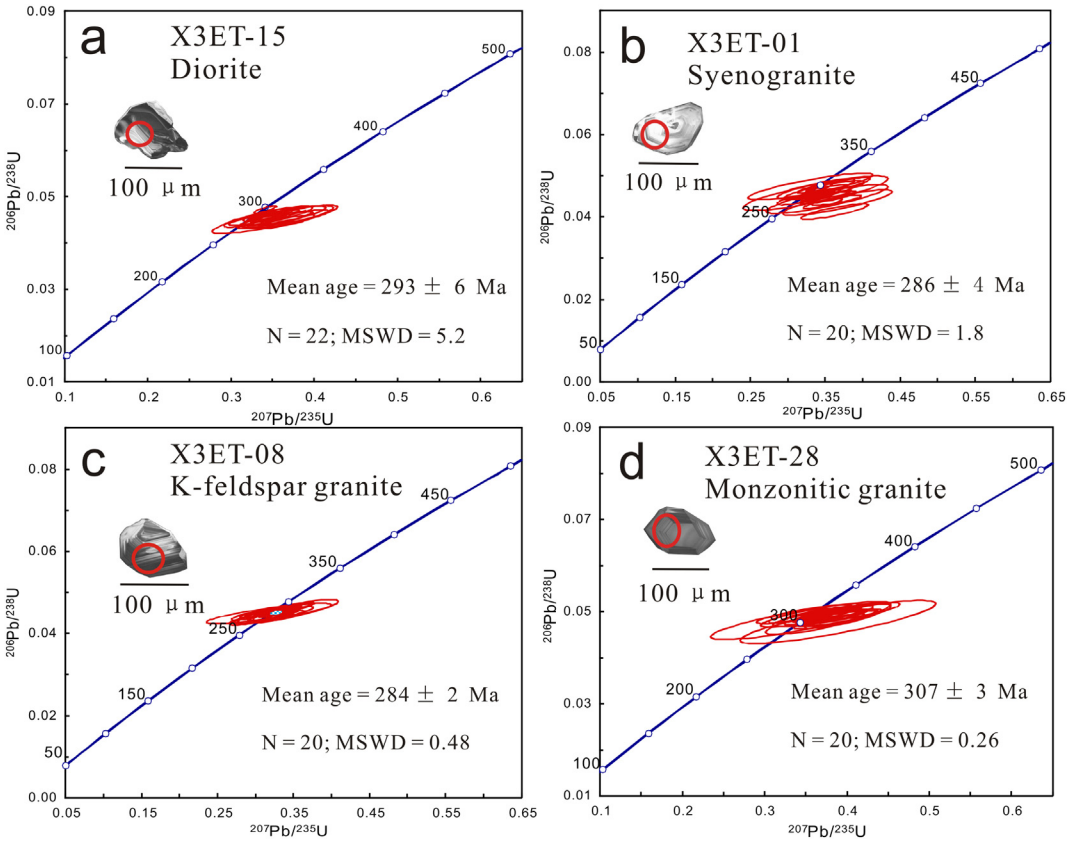


**Fig. 3.** Concordant diagrams of zircons from the Late Paleozoic rocks in the eastern Central Tianshan Block.

(1.64–1.76 wt%), total alkali ($K_2O + Na_2O$ = 5.76–6.19 wt%) and $K_2O/Na_2O$ (0.34–0.46), showing medium-K to high-K calc–alkaline characteristics (Fig. 4a–c). These samples are metaluminous with low ASI (aluminium saturation index: molar $Al_2O_3/(Na_2O + K_2O + CaO)$) values ranging from 0.71 to 0.74 (Fig. 4d). In the Chondrite-normalized diagram, they are characterized by LREE enrichment ($(La/Yb)_N$ = 8.08–8.74), with significant depletion of HREE ($(Gd/Yb)_N$ = 1.76–1.89) and weak to nil negative Eu anomalies ($Eu/Eu^*$ = 0.91–0.97), except for one sample (X3ET-19) showing relatively remarkable negative Eu anomalies ($Eu/Eu^*$ = 0.78) (Fig. 5a). These rocks have relatively high large ion lithophile element (LILE) concentrations, such as Ba (611–867 ppm) and Sr (537–690 ppm). They have moderate Cr (49.8–83.9 ppm), Co (26.4–31.5 ppm) and Ni (22.8–36.3 ppm) contents. In a primitive mantle normalized diagram, these samples show Nb, Ta and Ti negative anomalies, and display positive Rb, Ba and Pb anomalies (Fig. 5b). They have consistent initial $^{87}Sr/^{86}Sr$ ratios (0.7055) and a narrow range of $\varepsilon_{Nd}(t)$ values (−4.11 to −4.59), with Mesoproterozoic two stage Nd model ages ($T^2_{DM}$ = 1.41 to 1.45 Ga) (Supplemental Table S3).

#### 4.2.2. Syenogranites and K-feldspar granites

Samples from the syenogranitic and K-feldspar granitic plutons show similar geochemical characteristics of major and trace element, as well as Sr–Nd isotopic ratios (Supplemental Tables S2 and S3). They have coherent $SiO_2$ (75.5–76.2 wt%), $TiO_2$ (0.11–0.15 wt%), $Al_2O_3$ (12.2–12.6 wt%), $Fe_2O_3^T$ (1.08–1.90 wt%), MgO (0.05–0.16 wt%) and $K_2O$ (4.60–4.88 wt%) contents. These samples show high-K calc-alkaline characteristics (Fig. 4a–c). They are weakly metaluminous to weakly peraluminous with ASI values 0.98 to 1.04 (Fig. 4d). In the Chondrite-normalized plot, they show LREE-enriched ($(La/Yb)_N$ = 4.97–6.35) with flat HREE patterns ($(Ga/Yb)_N$ = 0.80–1.10) and remarkably negative Eu anomalies ($Eu/Eu^*$ = 0.10–0.15) (Fig. 5c). They have high Rb (228–267 ppm), Zr (295–411 ppm), Hf (8.43–17.8 ppm), Ce (70.5–124 ppm), Y (31.9–77.8 ppm) and Ga (25.1–27.8 ppm), with extremely low Sr (<30.9 ppm) and Eu (<0.41 ppm) concentrations, thus with high Rb/Sr (7.56–17.3) and 10,000 * Ga/Al (3.86–4.24) ratios. In a primitive mantle normalized diagram, they show strong negative Ba, Nb, Ta, Sr and Ti anomalies, and display positive Rb and Pb anomalies (Fig. 5d). The rocks with high Rb/Sr ratios usually yield highly variable $(^{87}Sr/^{86}Sr)_i$ values. In accordance with their Rb/Sr ratios, the studied syenogranitic and K-feldspar granitic plutons show abnormally low initial $^{87}Sr/^{86}Sr$ ratios (0.6707–0.6980), implying significant decoupling between Sr and Nd isotopes. The decoupling between Sr and Nd isotopes analogous to those of the A-type granites in the Lachlan Fold Belt and the Balikun area of Eastern Tianshan (King et al., 1997; Yuan et al., 2010). These samples have $\varepsilon_{Nd}(t)$ (−4.01 to −4.40) and two stage Nd model ages ($T^2_{DM}$ = 1.40 to 1.43 Ga) similar to the dioritic samples (Supplemental Table S3).

#### 4.2.3. Monzonitic granites

The monzonitic granitic samples have high $SiO_2$ (71.5–72.2 wt%) and $K_2O$ (5.04–5.34 wt%), but display low $Fe_2O_3^T$ (2.44–2.52 wt%) and MgO (0.40–0.47 wt%) contents, and thus have high $K_2O/Na_2O$ ratios (1.30–1.54) (Supplemental Table S2). They show high-K calc-alkaline characteristics similar to the Early Permian granitic rocks (Fig. 4a–c), but exhibit weakly metaluminous characteristics (ASI values = 0.92 to 1) (Fig. 4d) different from those of the Early Permian granitic samples. The monzonitic granites show remarkably LREE-enriched ($(La/Yb)_N$ = 11.4–12.2) and negative Eu anomalies ($Eu/Eu^*$ = 0.31–0.34), with relatively slightly depletion of HREE ($(Ga/Yb)_N$ = 1.71–1.76) (Fig. 5e). They also have high Rb (209–221 ppm), Zr (266–323 ppm), Hf

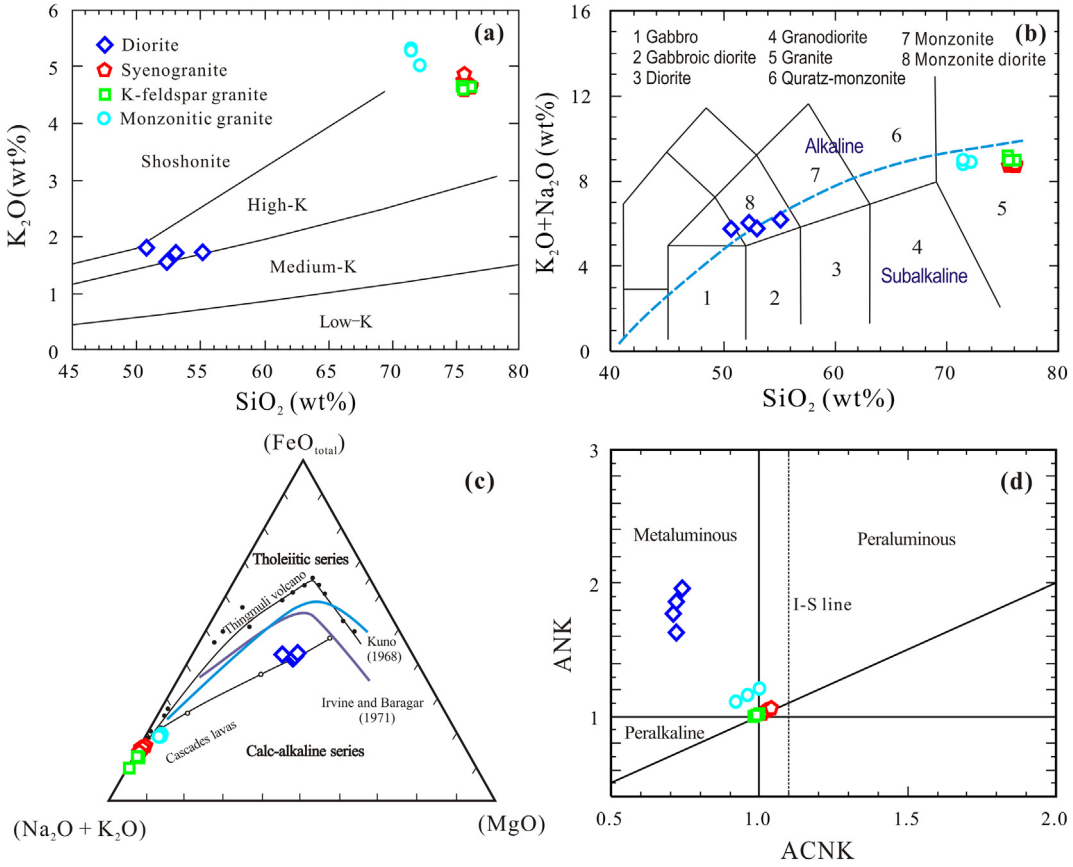


**Fig. 4.** Major element diagrams for the Late Paleozoic dioritic and granitic plutons. (a) $K_2O$ versus $SiO_2$ diagram; (b) TAS classification diagram; (c) AFM diagram with boundary between the calc-alkaline and tholeiitic fields; (d) ANK versus ACNK diagram.

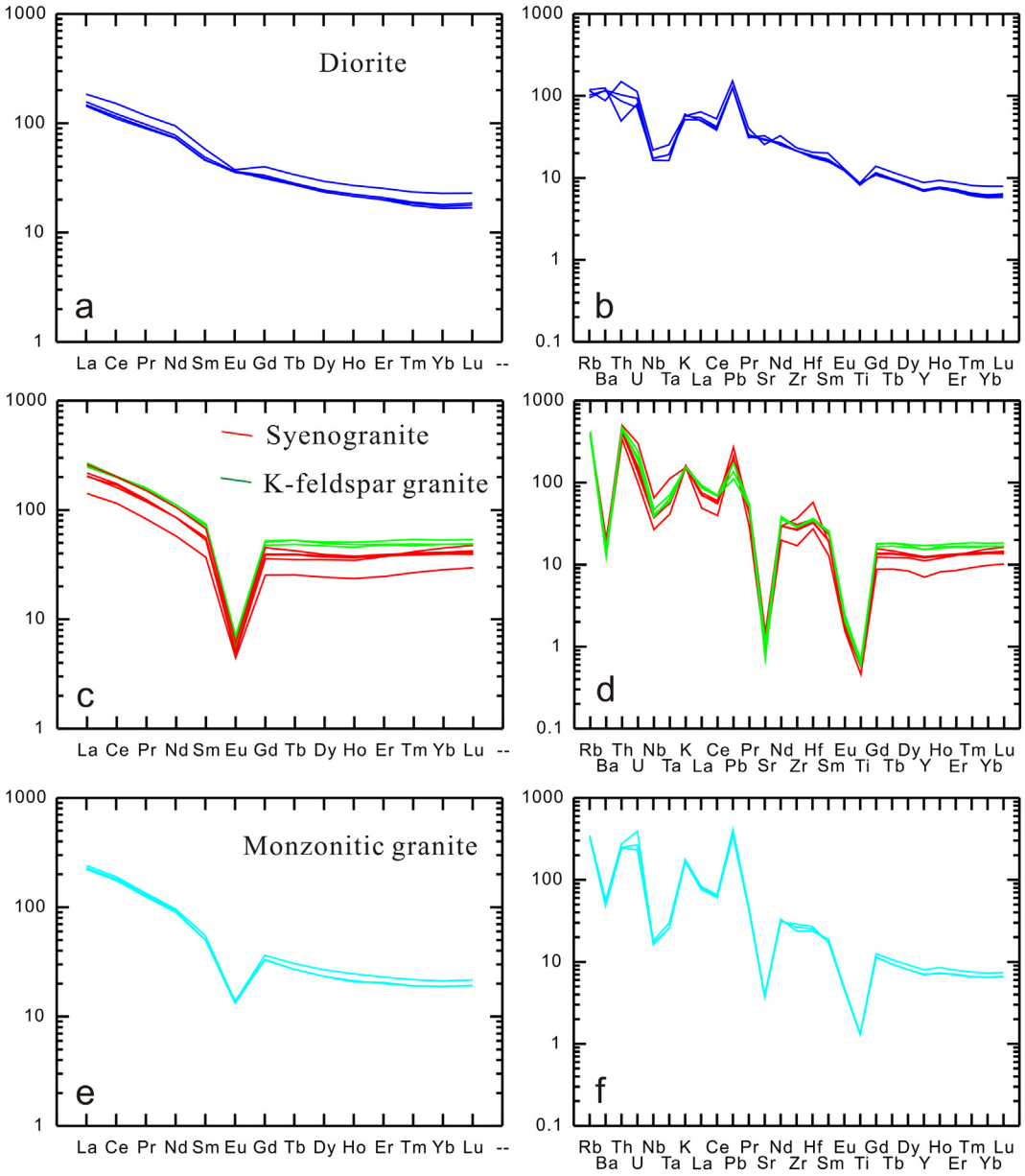


**Fig. 5.** Chondrite-normalized REE patterns (a, c and e) and Primitive mantle-normalized trace element spider diagrams (b, d and f). The data of Chondrite and Primitive Mantle are from Sun and McDonough (1989).

(7.30–8.32 ppm), Ce (108–116 ppm), Y (31.6–36.4 ppm) and Ga (18.6–20.3 ppm), but have low Sr (77.4–81.9 ppm) and Eu (0.77–0.81 ppm) concentrations, thus with high Rb/Sr (2.68–2.75) and 10,000 * Ga/Al (2.67–2.75) ratios, similar to the Early Permian granitic rocks. In a primitive mantle normalized diagram, they display strong negative Ba, Nb, Ta, Sr and Ti anomalies, and show positive Rb and Pb anomalies (Fig. 5f). These rocks have slight higher $\varepsilon_{Nd}(t)$ (−3.32) and more juvenile $T^2_{DM}$ ages (1.36 Ga) than the Early Permian dioritic and granitic intrusions (Supplemental Table S3).

## 5. Discussion

### 5.1. Petrogenesis of the diorites

The diorites are characterized by low $SiO_2$ (50.8–55.2 wt%), high MgO (4.3–5.3 wt%) and $Mg^{\#}$ (49–53), and relatively high Cr (49.8–83.9 ppm), Ni (22.8–36.3 ppm), V (177–206 ppm) concentrations, compared to the continental crust or crust-derived melts (Patiño Douce and Beard, 1995; Rudnick and Gao, 2003). These are indicative of a mantle component played a prominent role in their genesis (Tang et al., 2014; Wilson, 1989). Nevertheless, their $Mg^{\#}$ and Cr, Ni contents are much lower than those of typical mantle-derived primary melts ($Mg^{\#}$ = 73–81, Cr > 1000 ppm and Ni > 400 ppm) (Wilson, 1989), suggesting that they must have experienced various degrees of fractional crystallization from parental magmas either in the magma chambers or enroute to the surface (Chen et al., 2011; Zhang et al., 2016). A positive correlation between $Al_2O_3$, $Fe_2O_3^T$, Cr, Ni and MgO for the monzonite diorite rocks suggests fractionation of olivine and pyroxene (Supplemental Table S2). The depletions in Y and HREE of these samples require garnet or amphibole as early crystallizing phases. Fractionation of garnet can significantly increase the Dy/Yb ratios in the residual melt, whereas amphibole fractionation will cause a decrease in Dy/Yb rations with decreasing Mg# (Zhang et al., 2017 and references therein). The coherent Dy/Yb rations (1.93–2.11) of these rocks argue against the significant fractionation of amphibole or garnet. The lack of negative Sr and Eu anomalies in these samples suggests plagioclase

fractionation is limited, except for sample X3ET-19 which plagioclase fractionation is relatively significant, in accordance with its relatively low Sr (537 ppm, the other samples >600 ppm) concentration and negative Eu anomaly (Eu/Eu* = 0.78, the other samples = 0.91–0.97) (Fig. 5a–b). Negative Nb, Ta and Ti anomalies are obvious in the diorite samples, which could be the result of the Ti-bearing minerals fractionation (such as ilmenite and sphene), crustal contamination or their sources inheritance (Chen et al., 2011; Tang et al., 2014). However, their similar $TiO_2$ contents do not support fractionation of Ti-bearing minerals. Therefore, crustal contamination needs to be assessed for the dioritic samples before petrogenetic analysis.

Crustal contamination commonly appears to be a characteristic for mantle-derived magmas that ascend from their mantle sources through continental crust (Watson, 1982), but this was not a possible mechanism for the Early Permian diorites in this study. Since they have consistent $(^{87}Sr/^{86}Sr)_i$ values and give no correlated relationship between $(^{87}Sr/^{86}Sr)_i$ and 1/Sr (or $SiO_2$ and MgO) (Sun and McDonough, 1989; Wood, 1980). Furthermore, they have relatively high Ti/Zr (42.8–46.7) and Ti/Y (280–359) ratios, much higher than those of the typical crustal rocks (Ti/Zr < 30, Ti/Y < 200) (Wedepohl, 1995). Conclusively, the trace elements and similar isotope compositions of these samples have not been significantly modified by crustal contamination and thus can be used to constrain the nature of their mantle sources (Shellnutt et al., 2009; Zhang et al., 2016).

The diorite samples have Ta/Yb ratios (0.23–0.27) and Nb/Yb ratios (4–4.21) higher than *E*-MORB (0.2 and 0.02) (Sun and McDonough, 1989), suggesting a fertile mantle source (Pearce et al., 2005). An enriched component in basalt has been ascribed to OIB involvement (Márquez et al., 1999), asthenosphere upwelling (Ferrari, 2004), or enriched bands or streaks within depleted mantle domain, which resulted from the addition of low-degree melts prior to the main melting event (Yuan et al., 2010 and references therein). Their relatively higher Zr/Nb ratios (16.8–20.8) than OIB (5.8) (Sun and McDonough, 1989), but relatively low Nb/Yb ratios (4–4.21) (Fig. 6) exclude an OIB-derived origin. Metasomatism of depleted mantle by low amounts of partial melting would lead to superchondritic Nb/Ta ratios (Kalfoun et al., 2002). This is not consistent with the diorite samples which show subchondritic Nb/Ta ratios (<17.5), and argues against a mantle source metasomatised by low-degree melts. In the Th/Yb vs. Nb/Yb diagram (Fig. 6), all the diorite samples plot in the continental arc field and above the MORB-OIB array, suggesting the involvement of a continental arc or recycled crustal components (Pearce, 2008). A continental margin arc was suggested to have developed on the Precambrian basement of the Central Tianshan Block and the Late Carboniferous arc magmas were considered as the latest arc magmatism in the eastern Central Tianshan Block (Zhang et al., 2016). The recycled crustal components in the study area are dominated by the Precambrian crust of the Central Tianshan Block (Zhang et al., 2016). These diorite samples have negative $\varepsilon_{Nd}(t)$ values (−4.11 to −4.59) and relatively old two stage Nd model ages ($T^2_{DM}$ = 1.41 to 1.45 Ga), which indicate that the enrichment was caused by involvements of old crustal materials into the magma source and the Mesoproterozoic metamorphic rocks of the Central Tianshan Block were most likely to be the recycled crustal components. Their Sr–Nd isotopic compositions are distinctly different from the contemporaneous mafic–ultramafic (or intermediate) intrusions (Fig. 7a, b; Chai et al., 2008; Chen et al., 2013; Zhang et al., 2016), implying the feasibility of old crustal components. For example, there are 1.2–1.3 Ga metasedimentary rocks of the Xingxingxia group (Li et al., 2003), a 1.4 Ga granitic gneiss in the Bingdaban area (Chen et al., 2009), a 1.45 Ga granitic gneiss in the Xingxingxia area (Shi et al., 2010). The Sr–Nd isotopic compositions of the diorite samples similar to those of the Early Carboniferous Caixiashan mafic dikes in the Central Tianshan Block (Fig. 7a, b; Li et al., 2016) further support the input of old crustal materials into the magma source.

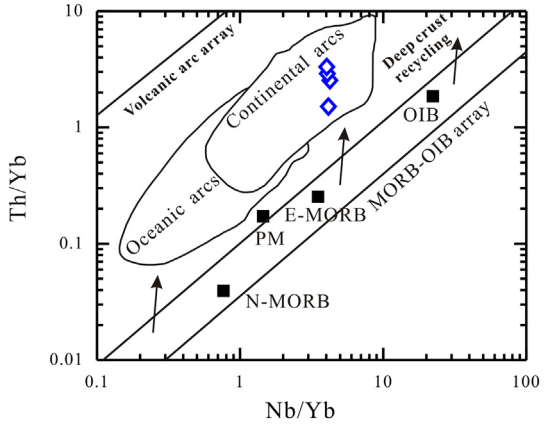


**Fig. 6.** Th/Yb vs. Nb/Yb correlation diagram for the Early Permian dioritic intrusion from the eastern Central Tianshan Block (after Pearce, 2008). Data for Primitive Mantle, N-MORB, *E*-MORB and OIB are from Sun and McDonough (1989). Symbols are same as Fig. 4.

Three of these samples have high Sr (609–690 ppm) contents and low HREE, with significant depletion of HREE ($(Gd/Yb)_N$ = 1.86–1.89) and weak to nil Eu anomalies (Eu/Eu* = 0.91–0.97), probably reflect the presence of garnet (Patiño Douce, 1996; Yuan et al., 2007 and references therein). The rest one sample with significant depletion of HREE ($(Gd/Yb)_N$ = 1.76), but relatively remarkable Eu anomalies (Eu/Eu* = 0.78), suggest the presence of both garnet and plagioclase (Patiño Douce, 1996; Yuan et al., 2007 and references therein). Recent experiments and case studies have revealed that the minimum pressure for garnet appearance is 0.8 to 1.0 GPa, the minimum pressure for plagioclase disappearance is 1.2 GPa (Xiong et al., 2005). Therefore, we conclude that the dioritic pluton may originate from a relatively fertile mantle at a shallow depth (0.8 to 1.2 GPa) induced by an upwelling asthenosphere in an extensional geodynamic setting. The mantle-derived primary magma compositions were modified by the old crustal materials added into the magma source rather than by crustal contamination. They had experienced fractionation of olivine and pyroxene, with a limited degree of plagioclase fractionation.

### 5.2. Petrogenesis and magma source of the granites

Granitic rocks can be genetically divided into I-, S-, M-, and A-types according to their chemical compositions and source rocks (Bonin, 2007; Whalen et al., 1987). In general, A-type granites have higher $K_2O + Na_2O$, Fe/Mg, Ga/Al, HFSE (e.g. Zr and Hf) and lower CaO, Sr, Eu and Ba than I- and S-type granites (Bonin, 2007; Collins et al., 1982; King et al., 1997; Whalen et al., 1987). The significantly high HFSE, HREE and FeO/MgO ratios, and remarkably low Ba, Sr and Eu contents of all the granites (Supplemental Table S2) suggest that they have geochemical characteristics of A-type granites (Bonin, 2007; Eby, 1992; Pearce et al., 1984; Whalen et al., 1987). In addition, in the $(K_2O + Na_2O)/CaO$ vs. Zr + Nb + Ce + Y and Nb vs. 10,000 Ga/Al diagrams (Fig. 8a, b; Pearce et al., 1984; Whalen et al., 1987), all the granite samples are plotted in the A-type field. Because the granites in this study lack inherited zircon, their zircon saturation temperature calculated from bulk rock compositions can be used to provide minimum estimate of the temperature of the initially emplaced magma (Watson and Harrison, 1983). The calculated zircon saturation temperatures ($T_{Zr}$) for the monzonitic granites, syenogranites and K-feldspar granites are in the range of 826–835 °C, 806–876 °C, and 847–851 °C, respectively (Supplemental Table S2; Watson and Harrison, 1983). These values are distinctly higher than those of I-type granites (calculated average $T_{Zr}$ values for unfractionated I-type granites and fractionated I-type granites were 781 and 764 °C, respectively; Watson and Harrison, 1983; King et al., 1997), but consistent with those of A-type granites (calculated average $T_{Zr}$ values of A-type granites was 839 °C, Watson and Harrison, 1983; King et al., 1997), further suggest these granites are A-type granites.

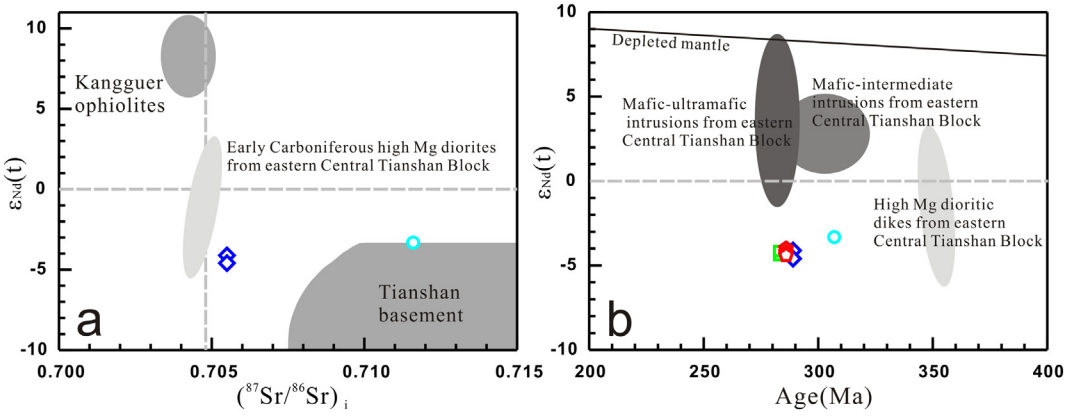


**Fig. 7.** (a) $\varepsilon_{Nd}(t)$ vs. $(^{87}Sr/^{86}Sr)_i$ diagram of the Late Paleozoic dioritic and granitic plutons from the eastern Central Tianshan Block. The data of Kangguer ophiolites are from Li et al. (2008). The data of high Mg diorites are from Li et al. (2016). The range of Tianshan basement is from Tang et al. (2014). (b) $\varepsilon_{Nd}(t)$ vs. Age (Ma) diagram of the Late Paleozoic dioritic and granitic plutons from the eastern Central Tianshan Block. The data of high Mg diorites are from Li et al. (2016). The data of mafic-intermediate intrusions are from Zhang et al. (2016). The data of mafic-ultramafic intrusions are from Chai et al. (2008) and Chen et al. (2013). Symbols are same as Fig. 4.

The petrogenesis and source of A-type granites are controversial (e.g. Bonin, 2007;Collins et al., 1982 ; Eby, 1990 ; King et al., 1997 ; Whalen et al., 1987). Several models have been proposed, including fractionation of mantle-derived magma (e.g. depleted mantle, or alkaline basic magmas; Bonin, 2007; Mao et al., 2014), partial melting of various crustal sources (Collins et al., 1982; Eby, 1990; King et al., 1997; Whalen et al., 1987), or mixing between mantle-derived magma and crustal melt (Bonin, 2007; Kemp et al., 2005). The major concerns of these models focus on the source regions and the role of the mantle (Wu et al., 2002; Yuan et al., 2010). If extensive fractional crystallization of mantle-derived magma took place, it would be expected large volumes mafic–intermediate rocks (Wu et al., 2002). However, very small proportion of contemporary mafic rocks in the study area indicate they cannot be products of mantle-derived magmas differentiation (Chai et al., 2008; Chen et al., 2013; Zhang et al., 2016). Considering the high $SiO_2$ (>71.5 wt%) and low MgO (<0.5 wt%) contents of these A-type granites, they were unlikely directly derived from the mantle (Bonin, 2007; Mao et al., 2014). Although these A-type granites may not be differentiation products of mantle-derived magmas, various degrees of fractional crystallization were responsible to explain the compositional variation of these granites. For instance, the presence of Sr, Eu and Ba negative anomalies in the A-type granites (Fig. 5c–f) are hence indicative of fractionation of both plagioclase and K-feldspar (Wu et al., 2002). The lack of inherited zircon or mafic microgranular enclaves in these granitic intrusions does not support the mixing between mantle-derived magma and crustal melts (Yuan et al., 2010). Although a mantle material contribution can be precluded, the heat contribution from mantle cannot be completely ruled out.

The rocks with high Rb/Sr ratios usually yield highly variable $(^{87}Sr/^{86}Sr)_i$ values, thus the $(^{87}Sr/^{86}Sr)_i$ values for such high Rb/Sr rocks cannot be used in petrogenetic discussions (Wu et al., 2002). Therefore, we use Nd isotopic composition to constrain magma source of these A-type granitic rocks. These A-type granites all have negative $\varepsilon_{Nd}(t)$ values (−3.32 to −4.40) and Mesoproterozoic two stage Nd model ages ($T^2_{DM}$ = 1.36 to 1.43 Ga) indicating a relatively old crustal source. The Mesoproterozoic metamorphic crustal rocks of the Central Tianshan Block is most likely to be the magma source for these A-type granites (Fig. 7).

A-type granites include not only typical peralkaline type, but also aluminous type (King et al., 1997; Shellnutt et al., 2009). For example, the peralkaline A-type granites in NE China contains alkali mafic minerals, such as arfvedsonite, riebeckite and sodium pyroxene, while the aluminous A-type granites in NE China have annite and/or calcic- or sodic-calcic amphibole as the mafic phase (Wu et al., 2002). King et al. (1997) suggested that the peralkaline A-type granites from the Lachlan Fold Belt were fractionation from a mafic source, but the aluminous type were generated by partial melting of a crustal source. Recently, some case studies also suggested that the aluminous A-type granites from South and East China were originated from crustal rocks (Li et al., 2013; Sun et al., 2011). The Late Carboniferous monzonitic granites are weakly metaluminous with A/CNK values ranging from 0.92 to 1 and A/NK values ranging from 1.11 to 1.21 (Fig. 4d), whereas the Early

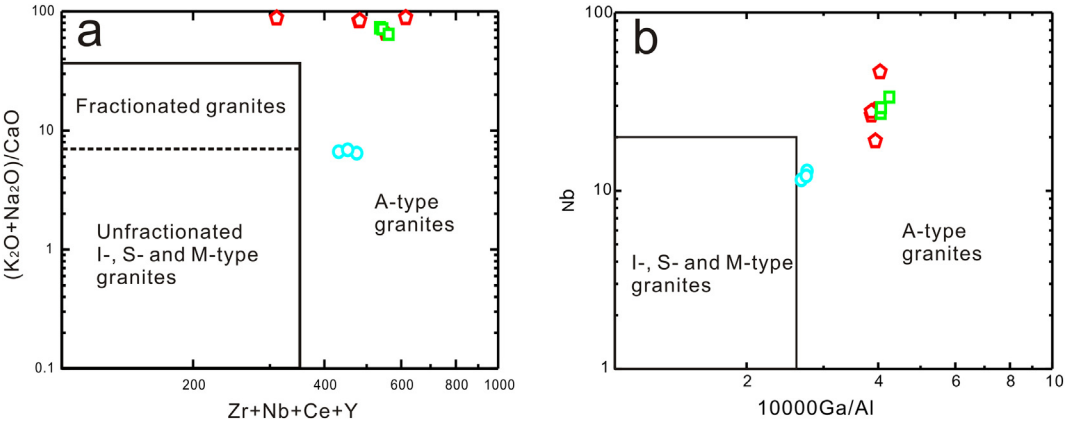


**Fig. 8.** (a) $(K_2O + Na_2O)/CaO$ vs. Zr + Nb + Ce + Y, (b) Nb vs. 10,000Ga/Al diagram for the Late Paleozoic granitic plutons (after Pearce et al., 1984; Whalen et al., 1987). Symbols are same as Fig. 4.

Permian syenogranites and K-feldspar granites are weakly metaluminous to weakly peraluminous with ASI values of 0.98–1.04 (Fig. 4d). The absence of alkali mafic minerals but occurrence of calcic amphibole in these granites (Fig. 2g–i) is agreement with a classification of aluminous A-type granites. Therefore, we suggest that the parental melts of these aluminous A-type granites were generated from Mesoproterozoic metamorphic basement rocks of the Central Tianshan Block.

The magma source of the aluminous A-type granites could be metasedimentary rocks or metaigneous rocks, or anhydrous lower crustal granulitic residues from which a granitic melt was previously extracted. Nevertheless, experimental petrology has suggested that a residual granulitic source is unlikely to be the source of the A-type granites since it is too refractory (e.g. Creaser et al., 1991). Additionally, partial melting of the metasedimentary rocks usually produce magmas with low alkaline contents and high $Al_2O_3$, exhibiting peraluminous character (e.g. Collins et al., 1982). The high alkaline signatures and low $Al_2O_3$ contents of all the studied granites (Fig. 4a–c), along with the absence of aluminium-rich minerals (such as muscovite and garnet) (Fig. 2g-i) and their metaluminous to weakly peraluminous features (Fig. 4d), are incompatible with the origin of metasedimentary source (Deng et al., 2016).

By contrast, these aluminous A-type granites having high $K_2O/Na_2O$ ratios, low CaO and $P_2O_5$ contents, and depletion in Sr and Eu (Supplemental Table S2), are similar to the experimental melt that was derived from partial melting of crustal metaigneous rocks at the depth of middle to lower crust levels (Patiño Douce, 1996). The Late Carboniferous monzonitic granites show slightly depletion of HREE ($(Ga/Yb)_N$ = 1.71–1.76) and display Eu, Sr negative anomalies (Fig. 5e–f), suggesting the present of both plagioclase and garnet in the magma source and the magma generation under a pressure of 0.8–1.2 GPa (Patiño Douce and Beard, 1995; Xiong et al., 2005). The Early Permian syenogranites and K-feldspar granites have relatively flat HREE patterns, which suggests the garnet was absent in the magma source and argues for magma generation under a pressure lower than 0.8–1.0 GPa (Patiño Douce and Beard, 1995; Xiong et al., 2005). In addition, the slight higher $\varepsilon_{Nd}(t)$ (−3.32) and more juvenile $T^2_{DM}$ ages (1.36 Ga) of the monzonitic granites than the syenogranites and K-feldspar granites ($\varepsilon_{Nd}(t)$ = −4.01 to −4.40; $T^2_{DM}$ = 1.40 to 1.43 Ga) suggest the different crustal source origin. Therefore, we conclude that the Late Carboniferous monzonitic granites were generated by partial melting of metaigneous rocks at a relatively deeper crustal level, whereas the Early Permian aluminous A-type granites were originated from a relatively shallow level.

### 5.3. Tectonic setting

In the eastern Central Tianshan Block, Late Carboniferous magmatic intrusions around 300 Ma are strikingly sparse and small in volume. This is distinctly different from widely distributed Carboniferous arc-related volcanic rocks or Early Permian post-collisional mafic and granitic intrusions (Chai et al., 2008; Chen et al., 2013; Deng et al., 2015; Li et al., 2016; Ma et al., 2015; Qin et al., 2011; Zhang et al., 2016; Zhao et al., 2018). The Central Tianshan continental arc was suggested to have formed by the south-dipping of the North Tianshan Oceanic lithosphere (e.g. Lei et al., 2011; Windley et al., 1990), the latest arc magmatism was represented by the existence of 325–320 Ma arc-related granitic gneisses (Wang et al., 2018b; Zhao et al., 2018) and ca. 310 mafic intrusions in the Central Tianshan Block (Zhang et al., 2016), as well as ca. 335 Ma arc-related granites (Du et al., 2018b) along the northern margin of this Block (Fig. 10a). Such a Carboniferous arc system was further supported by the presence of ca. 330 ophiolites in the North Tianshan (Fig. 10b; Liu et al., 2016). The Early Permian post-collisional tectonic setting was evidenced by the widely distributed of mafic–ultramafic intrusions and granitoids in the eastern Central Tianshan (Fig. 10c; Chai et al., 2008; Chen et al., 2013; Deng et al., 2015; Ma et al., 2015; Zhang et al., 2016).

A-type granites were common in extensional tectonic regimes that were usually interpreted as post-collisional or intraplate extensional settings (e.g. Collins et al., 1982; Eby, 1990, 1992; Tang et al., 2014). Eby (1992) subdivided A-type granites into two sub-groups and suggested that they may have different origins. The $A_1$-type granites (Y/Nb < 1.2) representing the differentiates of mantle-derived magmas emplaced in continental rifts or other intraplate environments, whereas the $A_2$-type granites (Y/Nb > 1.2) derived from melting of continental crust or underplated mafic crust and emplaced in a variety of tectonic environments (e.g. back-arcs, post-collision, strike-slip and transcurrent faults etc.) that have been through a cycle of continent-continent collision or island-arc magmatism (Eby, 1992; Mao et al., 2014). All the A-type granites in this study have high Y/Nb ratios (1.68–2.84) and fall into the $A_2$ group on the Ce-Nb-Y diagram (Fig. 9a; Eby, 1992). Because the latest arc magmas in the eastern Central Tianshan Block was emplaced at ca. 310 Ma (Zhang et al., 2016), a back-arc setting seems unlikely. In addition, on the diagram of Rb vs. (Y + Nb) (Pearce et al., 1984; Whalen et al., 1987), our results fall within the post-collisional field (Fig. 9b), consistent with the result in Fig. 9a. As discussed earlier, all the A-type granites were generated by crustal partial melting, but differ in the melting deep level and zircon saturation temperatures. Taking into account the Late Carboniferous and Early Permian A-type granites in this study may form in a same tectonic setting, we prefer an initial extension in the Late Carboniferous and then regional post-collisional extension in the Early Permian (Fig. 10).

### 5.4. Geodynamic implications

The Early Permian extensive partial melting of crustal materials and occurrence of mafic intrusions in the Eastern Tianshan requires vast heat input and may reflect underplating of mafic magmas, but the emplacement mechanism of mafic magmas in this area is still debatable (Deng et al., 2015; Yuan et al., 2010). Recently, a mantle plume model has been proposed to account for the Eastern Tianshan mafic–ultramafic intrusions (e.g. Qin et al., 2011), because of the nearly contemporaneous (272–292 Ma) mafic–ultramafic intrusions and continental flood basalts discovered in the Tarim Block (Zhang et al., 2010). However, the geochemical characteristics of the diorites are distinct from those of the Early Permian Tarim basalts and mafic dikes. The dioritic intrusion in this study has low LREE contents and show strongly negative Nb, Ta and Ti anomalies (Fig. 5a–b), whereas the Early Permian Tarim basalts and mafic dikes show more fractionated REE patterns, without pronounced peaks at Nb, Ta and Ti (Wei et al., 2014). In addition, the A-type granites in this study exhibit zircon saturation temperatures ($T_{Zr}$ = 806–876 °C) (Supplemental Table S2) significantly lower than that of A-type granites related to the Emeishan plume ($T_{Zr}$ = 934–1053 °C) (Xu et al., 2001). Thus, these Late Carboniferous A-type granites and Early Permian dioritic and A-type granitic rocks were unlikely to have originated from the Tarim mantle plume.

A large-scale lithosphere delamination is an alternative model for these dioritic and granitic magmas. This model is characterized by the sinking of heavier lithosphere and subsequent upwelling of extensive hot asthenosphere, accompanied by crustal extension (Deng et al., 2015; Ma et al., 2015). Magmatism formed in this setting would be distributed widely, but the magmatic activity in the Eastern Tianshan distribute within a roughly E-W narrow zone that paralleled to the E-W direction faults (Fig. 1b; Yuan et al., 2010; Deng et al., 2015; Ma et al., 2015), which does not seem to fit this model. Such a geographic distribution of magmatic activity is more consistent with the slab breakoff model (Davies and von Blanckenburg, 1995), which has been tested in the Eastern Tianshan (Chen et al., 2011; Deng et al., 2015; Ma et al., 2015; Yuan et al., 2010) as well as some well-known orogens, such as the Alps and Dabie Mountains (Davies and von Blanckenburg, 1995), the Caledonides (Atherton and Ghani, 2002) and the Himalayas (Lee et al., 2009).

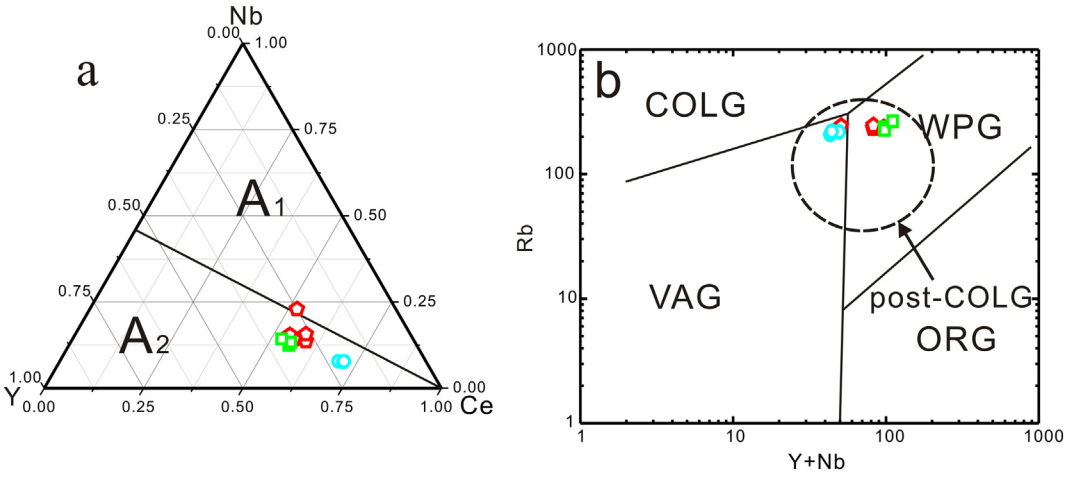


**Fig. 9.** (a) Y–Ce–Nb and (b) Rb vs. Y + Nb diagrams for the Late Paleozoic granitic plutons (after Pearce et al., 1984; Whalen et al., 1987). Abbreviations: COLG, collision granite; VAG, volcanic arc granite; ORG, ocean ridge granite; WPG, within plate granite; post-COLG, post collision granite.

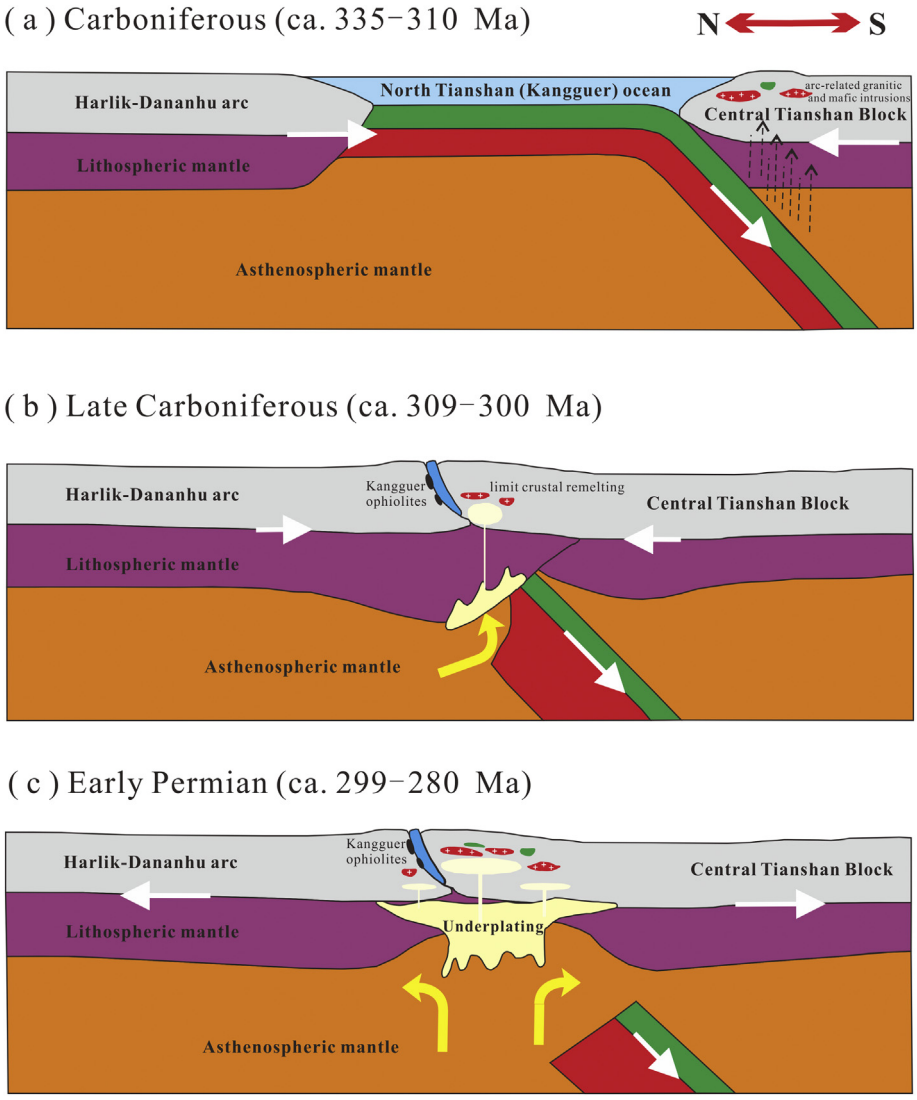


**Fig. 10.** Schematic diagrams of the Late Paleozoic evolution of the Eastern Tianshan (after Davies and von Blanckenburg, 1995; Yuan et al., 2010; Deng et al., 2015; Ma et al., 2015). (a) Lithosphere of the North Tianshan Ocean (namely Kangguer Ocean) south-dipping subducted beneath the Central Tianshan Block during the Carboniferous; (b) First stage of slab breakoff, resulting in limited mantle upwelling; (c) Last stage of slab breakoff, with the peak of mantle upwelling.

Slab breakoff can also cause upwelling of hot asthenosphere due to the crust extensional. This process can generate a thermal anomaly in the mantle wedge, giving rise to the melting of upwelling asthenosphere and overriding crustal materials (Davies and von Blanckenburg, 1995). Recent dynamic modeling studies have suggested that it commonly takes 8–30 Myr for a slab breakoff to complete in collisional settings (Gerya et al., 2004). Therefore, the relatively deep crustal melting and low zircon saturation temperatures ($T_{Zr}$ = 826–835 °C) for the Late Carboniferous (ca. 307 Ma) A-type granites probably suggest that the early stage of slab breakoff only generate a thermal anomaly in the mantle wedge and induced limit crustal remelting because of restricted mantle upwelling (Fig. 10b). With the slow increase in igneous activity and thermal anomaly associated with upwelling asthenospheric mantle, the slab breakoff completed in the Early Permian with the peak of mantle magma upwelling which was responsible for the formation of the studied dioritic and granitic intrusions and a large number of contemporaneous mafic–ultramafic intrusions and post-collisional granitic plutons in the Central Tianshan Block (Fig. 10c).

## 6. Conclusions

1. The syenogranitic and K-feldspar granitic plutons and the dioritic pluton were formed in the Early Permian, whereas the monzonitic granitic pluton was formed in the Late Carboniferous.

2. The dioritic pluton was produced by partial melting of a relatively fertile mantle modified by involvements of old crustal materials of the Central Tianshan Block. Its formation was induced by an upwelling asthenosphere in an extensional geodynamic setting.

3. All the granites exhibit characteristics of aluminous $A_2$-type granites. Late Carboniferous monzonitic granites were generated by partial melting of metaigneous rocks at a relatively deeper crustal level, whereas the Early Permian A-type granites were originated from partial melts of metaigneous rocks at a shallow level.

4. Formation of the A-type granites and diorites was triggered by a slab breakoff, which was initiated in the Late Carboniferous and ended in the Early Permian.

## Acknowledgements

We are very grateful to Editor for efficient editorial handling. Our paper has benefited from the constructive suggestions and comments of the anonymous referees, which have greatly improved the manuscript. This study was supported by National Basic Research Program of China (2014CB440801), National Natural Science Foundation of China (41421002, 41522202, and 41603028) and MOST Special Fund from the State Key Laboratory of Continental Dynamics.

## Appendix A. Supplementary data

Supplementary data to this article can be found online at https://doi.org/10.1016/j.lithos.2018.08.006.

## References

Atherton, M.P., Ghani, A.A., 2002. Slab breakoff: a model for Caledonian, late granite syncollisional magmatism in the orthotectonic (metamorphic) zone of Scotland and Donegal, Ireland. Lithos 62, 65–85.

BGMRXUAR (Bureau of Geology and Mineral Resources of Xinjiang Uygur Autonomous Region), 1993. Regional Geology of Xinjiang Uygur Autonomous Region. Geological Publishing House, pp. 1–841 (in Chinese).

Bonin, B., 2007. A-type granites and related rocks: Evolution of a concept, problems and prospects. Lithos 97, 1–29.

Cai, K.D., Long, X.P., Chen, H.Y., Sun, M., Xiao, W.J., 2018. Accretionary and collisional orogenesis in the south domain of the western Central Asian Orogenic Belt (CAOB). Journal of Asian Earth Sciences 153, 1–8.

Cao, Y.C., Wang, B., Jahn, B.M., Cluzel, D., Shu, L.S., Zhong, L.L., 2017. Late Paleozoic arc magmatism in the southern Yili Block (NW China): insights to the geodynamic evolution of the Balkhash-Yili continental margin, Central Asian Orogenic Belt. Lithos 278, 111–125.

Chai, F.M., Zhang, Z.C., Mao, J.W., Dong, L.H., Zhang, Z.H., Wu, H., 2008. Geology, petrology and geochemistry of the Baishiquan Ni-Cu-bearing mafic-ultramafic intrusions in Xinjiang, NW China: implications for tectonics and genesis of ores. Journal of Asian Earth Sciences 32, 218–235.

Charvet, J., Shu, L.S., Laurent-Charvet, S., 2007. Paleozoic structural and geodynamic evolution of eastern Tianshan (NW China): welding of the Tarim and Junggar plates. Episodes 30, 162–186.

Charvet, J., Shu, L.S., Laurent-Charvet, S., Wang, B., Faure, M., Cluzel, D., Chen, Y., Jong, K.D., 2011. Palaeozoic tectonic evolution of the Tianshan belt, NW China. Science China-Earth Sciences 54, 166–184.

Chen, X.Y., Wang, Y.J., Sun, L.H., Fan, W.M., 2009. Zircon SHRIMP U–Pb dating of the granitic gneisses from Bingdaban and Laerdundaban (Tianshan Orogen) and their geological significances. Geochimica 38, 424–431 (in Chinese with English abstract).

Chen, X.J., Shu, L.S., Santosh, M., 2011. Late Paleozoic post-collisional magmatism in the Eastern Tianshan Belt, Northwest China: new insights from geochemistry, geochronology and petrology of bimodal volcanic rocks. Lithos 127, 581–598.

Chen, B., He, J.B., Chen, C.J., Muhetaer, Z., 2013. Nd-Sr-Os isotopic data of the Baishiquan mafic-ultramafic complex from East Tianshan, and implications for petrogenesis. Acta Petrologica Sinica 29, 294–302 (in Chinese with English abstract).

Collins, W.J., Beams, S.D., White, A.J.R., Chappell, B.W., 1982. Nature and origin of A-type granites with particular reference to southeastern Australia. Contributions to Mineralogy and Petrology 80, 189–200.

Creaser, R.A., Price, R.C., Wormald, R.J., 1991. A-type granites revisited: assessment of a residual-source model. Geology 19, 163–166.

Davies, J.H., von Blanckenburg, F., 1995. Slab breakoff: a model of lithosphere detachment and its test in the magmatism and deformation of collisional orogens. Earth and Planetary Science Letters 129, 85–102.

Deng, Y.F., Song, X.Y., Hollings, P., Zhou, T.F., Yuan, F., Chen, L.M., Zhang, D.Y., 2015. Role of asthenosphere and lithosphere in the genesis of the Early Permian Huangshan mafic-ultramafic intrusion in the Northern Tianshan, NW China. Lithos 227, 241–254.

Deng, X.Q., Zhao, T.P., Peng, T.P., 2016. Age and geochemistry of the early Mesoproterozoic A-type granites in the southern margin of the North China Craton: constraints on their petrogenesis and tectonic implications. Precambrian Research 283, 68–88.

Du, L., Long, X.P., Yuan, C., Zhang, Y.Y., Huang, Z.Y., Sun, M., Zhao, G.C., Xiao, W.J., 2018a. Early Paleozoic dioritic and granitic plutons in the Eastern Tianshan Orogenic Belt, NW China: constraints on the initiation of a magmatic arc in the Southern Central Asian Orogenic Belt. Journal of Asian Earth Sciences 153, 139–153.

Du, L., Long, X.P., Yuan, C., Zhang, Y.Y., Huang, Z.Y., Wang, X.Y., Yang, Y.H., 2018b. Mantle contribution and tectonic transition in the Aqishan-Yamansu Belt, Eastern Tianshan, NW China: insights from geochronology and geochemistry of Early Carboniferous to Early Permian felsic intrusions. Lithos 304, 230–244.

Eby, G.N., 1990. The A-type granitoids—a review of their occurrence and chemical characteristics and speculations on their petrogenesis. Lithos 26, 115–134.

Eby, G.N., 1992. Chemical subdivision of the A-type granitoids: petrogenetic and tectonic implications. Geology 20, 641–644.

Ferrari, L., 2004. Slab detachment control on mafic volcanic pulse and mantle heterogeneity in Central Mexico. Geology 32, 77–80.

Gao, J., Klemd, R., 2003. Formation of HP–LT rocks and their tectonic implications in the western Tianshan Orogen, NW China: geochemical and age constraints. Lithos 66, 1–22.

Gao, J., Li, M.S., Xiao, X.C., Tang, Y.Q., He, G.Q., 1998. Paleozoic tectonic evolution of the Tianshan Orogen, northwestern China. Tectonophysics 287, 213–231.

Gao, J., Qian, Q., Long, L.L., Zhang, X., Li, J.L., Su, W., 2009. Accretionary orogenic process of Western Tianshan, China. Geological Bulletin of China 28, 1804–1816 (in Chinese with English abstract).

Gao, J., Klemd, R., Qian, Q., Zhang, X., Li, J.L., Jiang, T., Yang, Y.Q., 2011. The collision between the Yili and Tarim blocks of the Southwestern Altaids: geochemical and age constraints of a leucogranite dike crosscutting the HP-LT metamorphic belt in the Chinese Tianshan Orogen. Tectonophysics 499, 118–131.

Gerya, T.V., Yuen, D.A., Maresch, W.V., 2004. Thermomechanical modelling of slab detachment. Earth and Planetary Science Letters 226, 101–116.

Han, Y.G., Zhao, G.C., 2017. Final amalgamation of the Tianshan and Junggar orogenic collage in the southwestern Central Asian Orogenic Belt: constraints on the closure of the Paleo-Asian Ocean. Earth-Science Reviews https://doi.org/10.1016/j.earscirev.2017.09.012.

Han, B.F., Guo, Z.J., Zhang, Z.C., Zhang, L., Chen, J.F., Song, B., 2010. Age, geochemistry, and tectonic implications of a late Paleozoic stitching pluton in the North Tian Shan suture zone, western China. Geological Society of America Bulletin 122, 627–640.

Han, B.F., He, G.Q., Wang, X.C., Guo, Z.J., 2011. Late Carboniferous collision between the Tarim and Kazakhstan-Yili terranes in the western segment of the South Tian Shan Orogen, Central Asia, and implications for the Northern Xinjiang, western China. Earth-Science Reviews 109, 74–93.

Han, Y.G., Zhao, G.C., Sun, M., Eizenhofer, P.R., Hou, W.Z., Zhang, X.R., Liu, D.X., Wang, B., Zhang, G.W., 2015. Paleozoic accretionary orogenesis in the Paleo-Asian Ocean: insights from detrital zircons from Silurian to Carboniferous strata at the northwestern margin of the Tarim Craton. Tectonics 34, 334–351.

Han, Y.G., Zhao, G.C., Sun, M., Eizenhofer, P.R., Hou, W.Z., Zhang, X.R., Liu, Q., Wang, B., Liu, D.X., Xu, B., 2016. Late Paleozoic subduction and collision processes during the amalgamation of the Central Asian Orogenic Belt along the South Tianshan suture zone. Lithos 246, 1–12.

He, Z.Y., Zhang, Z.M., Zong, K.Q., Xiang, H., Chen, X.J., Xia, M.J., Xia, M.J., 2014. Zircon U–Pb and Hf isotopoc studies of the Xingxingxia Complex from the Eastern Tianshan (NW China): significance to the reconstruction and tectonics of the southern Central Asian Orogenic Belt. Lithos 190, 485–499.

Hu, A.Q., Zhang, G.X., Zhang, Q.F., Chen, Y.B., 1998. Constraints on the age of basement and crustal growth in Tianshan Orogen by Nd isotopic composition. Science in China Series D-Earth Sciences 41, 648–657.
Huang, Z.Y., Long, X.P., Wang, X.C., Zhang, Y.Y., Du, L., Yuan, C., Xiao, W.J., 2017. Precambrian evolution of the Chinese Central Tianshan Block: constraints on its tectonic affinity to the Tarim Craton and responses to supercontinental cycles. Precambrian Research 295, 24–37.
Kalfoun, F., Ionov, D., Merlet, C., 2002. HFSE residence and Nb/Ta ratios in metasomatised, rutile-bearing mantle peridotites. Earth and Planetary Science Letters 199, 49–65.
Kemp, A.I.S., Wormald, R.J., Whitehouse, M.J., Price, R.C., 2005. Hf isotopes in zircon reveal contrasting sources and crystallization histories for alkaline to peralkaline granites of Temora, southeastern Australia. Geology 33, 797–800.
King, P.L., White, A.J.R., Chappell, B.W., Allen, C.M., 1997. Characterization and origin of aluminous A-type granites from the Lachlan Fold Belt, southeastern Australia. Journal of Petrology 38, 371–391.
Kröner, A., Windley, B.F., Badarch, G., Tomurtogoo, O., Hegner, E., Jahn, B.M., Gruschka, S., Khain, E.V., Wingate, M.T.D., 2007. Accretionary growth and crust formation in the Central Asian Orogenic Belt and comparison with the Arabian–Nubian shield. Geological Society of America Memoirs 200, 181–209.
Lee, H.Y., Chung, S.L., Lo, C.H., Ji, J.Q., Lee, T.Y., Qian, Q., Zhang, Q., 2009. Eocene Neotethyan slab breakoff in southern Tibet inferred from the Linzizong volcanic record. Tectonophysics 477, 20–35.
Lei, R.X., Wu, C.Z., Gu, L.X., Zhang, Z.Z., Chi, G.X., Jiang, Y.H., 2011. Zircon U–Pb chronology and Hf isotope of the Xingxingxia granodiorite from the Central Tianshan zone (NW China): implications for the tectonic evolution of the southern Altaids. Gondwana Research 20, 582–593.
Li, Q.G., Liu, S.W., Han, B.F., Zhang, J., Chu, Z.Y., 2003. Nd isotopic characteristics of Proterozoic metasedimentary rocks and constraints on their provenance in the eastern segment of Central Tianshan Belt, Xinjiang. Progress in Natural Science 13, 908–913.
Li, W.Q., Ma, H.D., Wang, R., Wang, H., Xia, B., 2008. SHRIMP dating and Nd–Sr isotopic tracing of Kanggurtage ophiolite in eastern Tianshan, Xinjiang. Acta Petrologica Sinica 4, 773–780 (in Chinese with English abstract).
Li, Z.L., Zhou, J., Mao, J.R., Santosh, M., Yu, M.G., Li, Y.Q., Hu, Y.Z., Langmuir, C.H., Chen, Z.X., Cai, X.X., Hu, Y.H., 2013. Zircon U–Pb geochronology and geochemistry of two episodes of granitoids from the northwestern Zhejiang Province, SE China: implication for magmatic evolution and tectonic transition. Lithos 179, 334–352.
Li, D.F., Zhang, L., Chen, H.Y., Hollings, P., Cao, M.J., Fang, J., Wang, C.M., Lu, W.J., 2016. Geochronology and geochemistry of the high Mg dioritic dikes in Eastern Tianshan, NW China: geochemical features, petrogenesis and tectonic implications. Journal of Asian Earth Sciences 115, 442–454.
Liu, S.W., Guo, Z.J., Zhang, Z.C., Li, Q.G., Zheng, H.F., 2004. Nature of the Precambrian metamorphic blocks in the eastern segment of Central Tianshan: constraint from geochronology and Nd isotopic geochemistry. Science in China Series D: Earth Sciences 47, 1085–1094.
Liu, W.G., Zhang, J.D., Zhao, H.L., 2016. Geological Characteristics and geochronology of Dongdagou oceanic crust remmants in Eastern Tianshan, Xinjiang. Western Exploration Engineering 6, 130–133 (in Chinese).
Ma, X.X., Shu, L.S., Meert, J.G., 2015. Early Permian slab breakoff in the Chinese Tianshan belt inferred from the post-collisional granitoids. Gondwana Research 27, 228–243.
Mao, Q.G., Xiao, W.J., Fang, T.H., Windley, B.F., Sun, M., Ao, S.J., Zhang, J.E., Huang, X.K., 2014. Geochronology, geochemistry and petrogenesis of Early Permian alkaline magmatism in the Eastern Tianshan: implications for tectonics of the Southern Altaids. Lithos 190–191, 37–51.
Márquez, A., Oyarzun, R., Doblas, M., Verma, S.P., 1999. Alkalic (OIB-type) and calcalkalic volcanism in the Mexican volcanic belt: a case of plume-related magmatism and propagating rifting at an active margin? Geology 27, 51–54.
Patiño Douce, A.E., 1996. Effects of pressure and $H_2O$ content on the compositions of primary crustal melts. Transactions of the Royal Society of Edinburgh. Earth Science 87, 11–21.
Patiño Douce, A.E., Beard, J.S., 1995. Dehydration–melting of biotite and quartz amphibolite from 3 to 15 kb. Journal of Petrology 36, 707–738.
Pearce, J.A., 2008. Geochemical fingerprinting of oceanic basalts with applications to ophiolite classification and the search for Archean oceanic crust. Lithos 100, 14–48.
Pearce, J.A., Harris, N.B.W., Tindle, A.G., 1984. Trace element discrimination diagrams for the tectonic interpretation of granitic rocks. Jouraml of Petrology 25, 956–983.
Pearce, J.A., Stern, J.R., Bloomer, S.H., Fryer, P., 2005. Geochemical mapping of the Mariana arc-basin system: implications for the nature and distribution of subduction components. Geochemistry, Geophysics, Geosystems 6, 1–27.
Qin, K.Z., Sun, S., Li, J.L., Fang, T.H., Wang, S.L., Liu, W., 2002. Paleozoic epithermal Au and Cu deposits in North Xinjiang, China: epochs, features, tectonic linkage and exploration significance. Resource Geology 52, 291–300.
Qin, K.Z., Su, B.X., Sakyi, P.A., Tang, D.M., Li, X.H., Sun, H., Xiao, Q.H., Liu, P.P., 2011. SIMS zircon U–Pb geochronology and Sr–Nd isotopes of Ni-Cu-bearing mafic–ultramafic intrusions in Eastern Tianshan and Beishan in correlation with flood basalts in Tarim basin (NW China): constraints on a ca. 280 Ma mantle plume. American Journal of Science 311, 237–260.
Rudnick, R.L., Gao, S., 2003. Composition of the Continental Crust. 3. Elsevier-Pergamon, Oxford, pp. 1–64.
SengÖr, A.M.C., Natalin, B.A., Burtman, V.S., 1993. Evolution of the Altaid Tectonic Collage and Paleozoic crustal growth in Eurasia. Nature 364, 299–307.
Shellnutt, J.G., Wang, C.Y., Zhou, M.F., Yang, Y.H., 2009. Zircon Lu–Hf isotopic compositions of metaluminous and peralkaline A-type granitic plutons of the Emeishan large igneous province (SW China): constraints on the mantle source. Journal of Asian Earth Sciences 35, 45–55.
Shi, W.X., Liao, Q.A., Hu, Y.Q., Yang, Z.F., 2010. Characteristics of Mesoproterozoic granites and their geological significances from Middle Tianshan Block, East Tianshan District, NW China. Geological Science and Technology Information 29, 29–37 (in Chinese with English abstract).
Sun, S.S., McDonough, W.F., 1989. Chemical and isotopic systematics of oceanic basalts: implications for mantle composition and processes. Geological Society, London, Special Publications 42, 313–345.
Sun, Y., Ma, C.Q., Liu, Y.Y., She, Z.B., 2011. Geochronological and geochemical constraints on the petrogenesis of late Triassic aluminous A-type granites on Southeast China. Journal of Asian Earth Sciences 42, 1117–1131.
Tang, G.J., Chung, S.L., Wang, Q., Wyman, D.A., Dan, W., Chen, H.Y., Zhao, Z.H., 2014. Petrogenesis of a Late Carboniferous mafic dike–granitoid association in the western Tianshan: response to the geodynamics of oceanic subduction. Lithos 202–203, 85–89.
Wang, B., Cluzel, D., Shu, L.S., Faure, M., Charvet, J., Chen, Y., Meffre, S., de Jong, K., 2009. Evolution of calc-alkaline to alkaline magmatism through Carboniferous convergence to Permian transcurrent tectonics, western Chinese Tianshan. International Journal of Earth Sciences 98, 1275–1298.
Wang, B., Faure, M., Shu, L.S., de Jong, K., Charvet, J., Cluzel, D., Jahn, B.M., Chen, Y., Ruffet, G., 2010. Structural and geochronological study of high-pressure metamorphic rocks in the Kekesu Section (northwestern China): implications for the Late Paleozoic tectonics of the southern Tianshan. Journal of Geology 118, 59–77.
Wang, B., Shu, L.S., Faure, M., Jahn, B.M., Cluzel, D., Charvet, J., Chung, S.L., Meffre, S., 2011. Paleozoic tectonics of the southern Chinese Tianshan: insights from structural, chronological and geochemical studies of the Heiyingshan ophiolitic melange (NW China). Tectonophysics 497, 85–104.
Wang, B., Cluzel, D., Jahn, B.M., Shu, L.S., Chen, Y., Zhai, Y.Z., Branquet, Y., Barbanson, L., Sizaret, S., 2014. Late Paleozoic pre- and syn-kinematic plutons of the Kangguer-Huangshan shear zone: inference on the tectonic evolution of the eastern Chinese north Tianshan. American Journal of Science 314, 43–79.
Wang, B., Zhai, Y.Z., Kapp, P., Koen, K.D., Zhong, L.L., Liu, H.S., Ma, Y.Z., Gong, H.J., Geng, H.Y., 2018a. Accretionary tectonics of back-arc oceanic basins in the South Tianshan: insights from structural, geochronological, and geochemical studies of the Wuwamen ophiolite melange. Geological Society of America Bulletin 130, 284–306.
Wang, Y.F., Chen, H.Y., Han, J.S., Chen, S.B., Huang, B.Q., Li, C., Tian, Q.L., Wang, C., Wu, J.X., Chen, M.X., 2018b. Paleozoic tectonic evolution of the Dananhu-Tousuquan island arc belt, Eastern Tianshan: constraints from the magmatism of the Yuhai porphyry Cu deposit, Xinjiang, NW China. Journal of Asian Earth Sciences 153, 282–306.
Watson, E.B., 1982. Basalt contamination by continental crust: some experiments and models. Contributions to Mineralogy and Petrology 80, 73–87.
Watson, E.B., Harrison, T.M., 1983. Zircon saturation revisited: temperature and composition effects in a variety of crustal magma types. Earth and Planetary Science Letters 64, 295–304.
Wedepohl, K.H., 1995. The composition of the continental crust. Geochimica et Cosmochimica Acta 59, 1217–1232.
Wei, X., Xu, Y.G., Feng, Y.X., Zhao, J.X., 2014. Plume–lithosphere interaction in the generation of the Tarimlarge igneous province, NW China: geochronological and geochemical constraints. American Journal of Science 314, 314–356.
Whalen, J.B., Currie, K.L., Chappell, B.W., 1987. A-type granites: geochemical characteristics, discrimination and petrogenesis. Contributions to Mineralogy and Petrology 95, 407–419.
Wilson, M., 1989. Igneous Petrogenesis: A Global Tectonic Approach: London. Unwyn Hyman.
Windley, B.F., Allen, M.B., Zhang, C., Zhao, Z.Y., Wang, G.R., 1990. Paleozoic accretion and Cenozoic redeformation of the Chinese Tien Shan Range, Central Asia. Geology 18, 128.
Wood, D.A., 1980. The application of a Th-Hf-Ta diagram to problems of tectonomagmatic classification and to establishing the nature of crustal contamination of basaltic lavas of the British Tertiary volcanic province. Earth and Planetary Science Letters 50, 11–30.
Wu, Y.B., Zheng, Y.F., 2004. Study on zircon in mineralgeny and the constraints on the interpretation of U–Pb ages. Chinese Science Bulletin 49, 1589–1604 (in Chinese).
Wu, F.Y., Sun, D.Y., Li, H.M., Jahn, B.M., Wilde, S., 2002. A-type granites in northeastern China: age and geochemical constraints on their petrogenesis. Chemical Geology 287, 143–173.
Xiao, W.J., Windley, B.F., Sun, S., Li, J., Huang, B.C., Han, C.M., Yuan, C., Sun, M., Chen, H.L., 2015. A tale of amalgamation of three Permo-Triassic collage systems in Central Asia: oroclines, sutures, and terminal accretion. Annual Review of Earth and Planetary Sciences 43, 477–507.
Xiong, X.L., Adam, J., Green, T.H., 2005. Rutile stability and rutile/melt HFSE partitioning during partial melting of hydrous basalt: implications for TTG genesis. Chemical Geology 218, 339–359.
Xu, Y.G., Chung, S.L., Jahn, B.M., Wu, G.Y., 2001. Petrologic and geochemical constraints on the petrogenesis of Permian–Triassic Emeishan flood basalts in southwestern China. Lithos 58, 145–168.
Yuan, C., Sun, M., Xiao, W.J., Li, X.H., Chen, H.L., Lin, S.F., Xia, X.P., Long, X.P., 2007. Accretionary orogenesis of the Chinese Altai: Insights from Paleozoic granitoids. Chemical Geology 242, 22–39.
Yuan, C., Sun, M., Wilde, S., Xiao, W.J., Xu, Y.G., Long, X.P., Zhao, G.C., 2010. Post-collisional plutons in the Balikun area, East Chinese Tianshan: evolving magmatism in response to extension and slab break-off. Lithos 119, 269–288.
Zhang, C.L., Li, Z.X., Li, X.H., Xu, Y.G., Zhou, G., Ye, H.M., 2010. A Permian large igneous province in Tarim and Central Asian orogenic belt, NW China: results of a ca. 275 Ma mantle plume? Geological Society of America Bulletin 122, 2020–2040.

Zhang, X.R., Zhao, G.C., Eizenhöfer, P.R., Sun, M., Han, Y.G., Hou, W.Z., Liu, D.X., Wang, B., Liu, Q., Xu, B., Zhu, C.Y., 2016. Tectonic transition from Late Carboniferous subduction to Early Permian post-collisional extension in the Eastern Tianshan, NW China: insights from geochronology and geochemistry of mafic-intermediate intrusions. Lithos 256–257, 269–281.

Zhang, Y.Y., Yuan, C., Sun, M., Long, X.P., Wang, Y.P., Jiang, Y.D., Lin, Z.F., 2017. Arc magmatism associated with steep subduction: insights from trace element and Sr–Nd–Hf–B isotope systematics. Journal of Geophysical Research - Solid Earth 122 (3), 1816–1834.

Zhao, L.D., Chen, H.Y., Zhang, L., Zhang, W.F., Yang, J.T., Yan, X.L., 2018. The Late Paleozoic magmatic evolution of the Aqishan-Yamansu belt, Eastern Tianshan: constraints from geochronology, geochemistry and Sr-Nd-Pb-Hf isotopes of igneous rocks. Journal of Asian Earth Sciences 153, 170–192.